Charging Nanowalls: Adjusting the Carbon Nanotube Isoelectric Point via Surface Functionalization

ARTICLE *in* THE JOURNAL OF PHYSICAL CHEMISTRY C · AUGUST 2009

Impact Factor: 4.77 · DOI: 10.1021/jp901439g

Charging Nanowalls: Adjusting the Carbon Nanotube Isoelectric Point via Surface Functionalization

Martin R. McPhail, Jacob A. Sells,† Zhen He, and Charles C. Chusuei*

Chemistry Department, Missouri University of Science and Technology, 142 Schrenk Hall, 400 West 11th Street, Rolla, Missouri 65409-0010

Received: February 17, 2009; Revised Manuscript Received: June 5, 2009

Controlling the point of zero charge (PZC) of carbon nanotubes is important for depositing finely dispersed metal nanoparticles from precursors in solution for fabricating chemical and biological sensor and catalyst surfaces. HiPco single-walled carbon nanotubes (p-SWNTs) were functionalized with carboxylic acid (COOH-SWNT), nitroso (NO-SWNT), and maleic anhydride (MA-SWNT) groups. The presence of attached moieties on the carbon nanotube surface was verified using X-ray photoelectron (XPS) and attenuated total reflection infrared (ATR-IR) spectroscopies. PZC measurements (in parentheses) were in the descending order: NO-SWNTs (7.5) > p-SWNTs (3.5) > MA-SWNTs (2.0) > COOH-SWNTs (1.2). The trend in measured PZC values correlated with the electron withdrawing character of the attached moieties, consistent with Hammett σ constants. Variations in the electron withdrawing character of the moieties led to SWNTs with differing semiconducting character, as observed in the UV−vis-NIR E_{11} semiconducting region and Raman D-to-G band ratios. These results suggest a tunability of the SWNT PZC via sidewall functionalization, a factor to consider for practical SWNT nanomaterial fabrication.

Introduction

The ability to control Coulombic properties at the solid−liquid interface is important for depositing highly dispersed, metal nanoparticles (using ionic precursors) on carbon surfaces. Fabrication of these materials is important for fabricating chemical and biological sensors,[1−4] heterogeneous catalysts,[5−11] and fuel cell[12] supports. The point-of-zero charge (PZC) is the pH at which the solid surface is electrostatically neutral under aqueous solution conditions, depending on the ability of hydroxylated surfaces to become protonated or deprotonated, according to Gouy−Chapman theory.[13] Solid−water interfaces acquire a net charge of a particular sign to maintain electrical neutrality. A substrate placed in aqueous solutions below its PZC becomes protonated and adsorbs anions as the surface adopts a positive charge. In contrast, a surface placed in solutions above its PZC adopts a negative surface charge (from deprotonation) and adsorbs cations. Practical catalyst support fabrication involves adjusting the PZC to adsorb selected metal complex precursors and avoiding agglomeration of nanoparticles to achieve the desired structures. Prior attempts to control the PZC of carbon black supports have focused on controlling the extent of decorating the carbon surface with oxygen-containing functional groups.[14−18]

Carbon nanotubes, with their unique electronic and structural properties,[12,19,20] offer rich avenues for surface functionalization and, hence, a means for tuning the PZC. Metal oxides placed in aqueous solution environments (e.g., SiO_2, Al_2O_3, TiO_2, MgO, etc.) are known to have characteristic PZC values.[13] By analogy, carbon nanotube surfaces have a wide range of PZCs available through chemical functionalization. However, only a few studies to date[21,22] have probed the effects of tethering various moieties on the carbon nanotube PZC. In this study, we have functionalized HiPco single-walled carbon nanotubes (SWNTs) to produce carboxylic acid (COOH-SWNT), maleic anhydride (MA-SWNT), and nitroso (NO-SWNT) attached surfaces in order to examine the effects of the tethered groups on its electronic structure and PZC.

Experimental Section

Materials. HiPco "pristine" SWNTs (p-SWNTs; 99.9% purity) used for all functionalization reactions were acquired from Carbon Nanotechnologies Inc. (lot no. P0289; Houston, TX) and used as received. This lot consisted of 0.7 nm diameter SWNTs with molar masses ranging from 3.4×10^5 to 5.2×10^6 g/mol. It should be noted that the SWNTs used contained a mixture of metallic and semiconducting types, which were not separated. Other reagents at 99+% purity, potassium nitrite, chloroform, nitric acid, sulfuric acid, and maleic anhydride, were purchased from Aldrich Chemical Co. Standard purity (BOC Gases; 99.9% purity) N_2 and Ar gases were used to maintain inert atmosphere during the SWNT functionalization reactions and heating of the Triton X-100 treated SWNT sheets, respectively.

Procedure. (1) COOH-SWNTs were prepared by refluxing in H_2SO_4/HNO_3, as described elsewhere.[23] A 30.0 mL solution of 3:1 concentrated nitric-to-sulfuric acid ratio was added to a 100 mL round-bottom glass flask along with 60.1 mg of p-SWNTs. The mixture was refluxed at 338 K for 12 h, with constant magnetic stirring, under N_2 atmosphere. (2) NO-SWNTs were prepared using an electrochemical functionalization procedure based on that described by Wang et al.[24] SWNT sheets were prepared by sonicating in 1% Triton X-100 (The Chemistry Store.com Inc.; St. Cayce, SC) solution followed by vacuum filtration with Millipore Teflon filter paper (0.2 μm pore size). The solid was dried on the filter paper and lifted off as a single sheet to be used as a working electrode in the electrochemical functionalization. Remaining surfactant was removed

* To whom correspondence should be addressed. E-mail: chusuei@mst.edu. Phone: 573-341-4537. Fax: 573-341-6033.
† Contributing coauthor performed experiments as a high school junior (Rolla High School, Rolla, MO 65401).

10.1021/jp901439g CCC: $40.75
Published on Web 07/22/2009

by annealing at 120 °C for 2 h, 300 °C for 1 h, and 800 °C for 30 min under inert Ar atmosphere. Complete removal of the Triton X-100 required additional electrochemical oxidation of the nanotubes, which occurred during the nitrosylation. ATR-IR spectra, included in the Supporting Information section, verified complete removal of the Triton X-100 surfactant. Electrochemical nitrosylation took place in 6 M KNO_2 with an SWNT sheet as the working electrode, a Ag/AgCl reference electrode, and a Pt wire counter electrode. The system was sparged with Ar gas and run for 6 h at 2.0 V using a 273 EG&G Princeton Applied Research potentiostat. (3) The MA-SWNT adduct was prepared via Diels−Alder addition reaction with maleic anhydride as the dienophile,[25,26] in good agreement with ab initio predictions for Diels−Alder additions to SWNT sidewalls.[27] The synthesis involved adding 50.0 mg of the HiPco p-SWNTs to an excess of maleic anhydride dissolved in chloroform. This mixture was placed in a 100 mL round-bottom flask and refluxed at 323 K for 12 h, with constant stirring, under N_2 atmosphere. Infrared spectroscopy confirmed the identity of the resulting adduct (vide infra). All of the functionalization procedures were carried out for prolonged periods (12 h) to ensure saturation of the SWNTs with their respective moieties. The SWNTs were then recovered by vacuum filtration using a Buchner funnel and Fluoropore PTFE membrane filters with a 0.2 μm pore size. Samples were rinsed with copious amounts of Millipore H_2O. Samples were then dried in a vacuum desiccator and saved in glass vials for further analysis.

Surface Characterization. The solid surfaces of the dried SWNTs were characterized by attenuated total reflection infrared (ATR-IR) and X-ray photoelectron (XPS) spectroscopies. ATR-IR was conducted using a Nicolet Nexus 470 FT-IR instrument, having a resolution of 4 cm^{-1}. All of the SWNT samples studied were deposited as thin films on the surface of a ZnSe crystal by sonicating 4.0 mg amounts of the sample in 2.0 mL of Millipore water. This solution was applied to the ZnSe crystal and allowed to evaporate to create thin films for analysis. ATR-IR spectra were acquired under a dry N_2 purge. XPS was performed using an ion-pumped Perkin-Elmer PHI ESCA 560 system, equipped with a double pass cylindrical mirror analyzer, using a Mg Kα anode operating at 15 kV and 250 W with a photon energy of $h\nu = 1253.6$ eV. Samples were mounted using double-sided tape (3 M Scotch) and turbopumped in a Teflon sliding seals load-lock prior to introduction into ultrahigh vacuum. Photoelectron spectra were charge corrected using as a reference the C 1s core level at 284.4 eV, corresponding to graphitic carbon on the SWNT graphene sheets.[28,29] Pressures did not exceed $\sim 1 \times 10^{-8}$ Torr during scans. XPS data were curve fitted using CasaXPS VAMAS processing software ver. 2.2.107 (Devon, United Kingdom) with a Shirley background subtraction[30] and 70:30 Gaussian−Lorentzian line shapes. In order to validate the mechanism for the nitrosylation of the SWNTs, an aliquot of the remaining solution of the electrochemical cell after the electrochemical functionalization was pipetted onto a vacuum-annealed 0.1 mm × 1 cm × 1 cm Ta foil (99.9% purity, H. Cross Company). The droplet was allowed to dry in an N_2 environment prior to introduction to the antechamber for XPS scans.

Determination of Points of Zero Charge. Isoelectric point measurements at the solid−liquid interface were also made on the MA-SWNT, NO-SWNT, COOH-SWNT, and p-SWNT surfaces using a method described by Park and Regalbuto.[31] Twelve solutions in the range of pH = 1.0−12.0 were made using dilute aqueous solutions of NaOH and HCl. A 1.8 mL aliquot of each solution was pipetted into polyethylene vials and allowed to equilibrate for 1 h. The initial pH of each solution was then recorded. A 2.0 mg amount of the SWNTs to be examined were added to each vial, which was then capped and shaken with a vortex mixer to settle the SWNTs. After an additional 12 h equilibration period, the final pH at the SWNT solid surface was measured for each vial using a spear-tip semisolid electrode. Plots of initial versus final pH values reveal plateaus denoting PZCs for each SWNT sample.

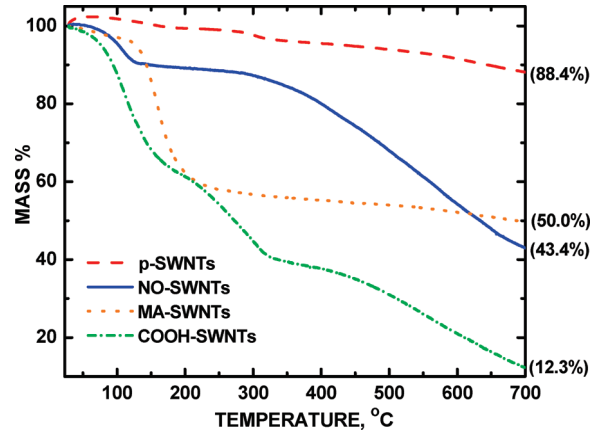

Figure 1. TGA of p-SWNTs, MA-SWNTs, NO-SWNTs, and COOH-SWNTs.

Optical Spectroscopy. UV−vis-NIR spectroscopy was performed using a CARY 5 spectrophotometer. Sample solutions were prepared by sonicating the SWNT sample in D_2O (99.8%, Cambridge Isotope Laboratories, Inc.) for several minutes. The resulting dispersions were diluted as necessary to give approximately equal scattering (in the 1200−1350 nm range) to normalize intensities in the E_{11} semiconducting band region for spectral comparison of the functionalized SWNT samples. Raman spectroscopy was carried out using a LabRAM Aramis Raman spectrometer with a HeNe laser (633 nm) and a D1 filter. The SWNTs were deposited onto 1 cm × 1 cm × 1 mm Si(100) substrates for Raman analysis, in which 1 mg amounts of the SWNTs of interest was placed in a polyethylene vial with two drops of Millipore water and sonicated. The resulting colloidal dispersion was dropped onto the Si(100) substrate and allowed to air-dry overnight, prior to analysis. All samples were read at several positions to ensure accuracy. The Raman transition for the underlying Si(100) at 516 nm was seen for all samples and used to ensure measurement accuracy.

Thermogravimetric Analysis (TGA). TGA was performed on all functionalized as well as plain SWNTs using a thermoanalyzer apparatus (Netzsch STA 409C/CD). The analysis was performed in N_2 atmosphere with a heating rate of 10 °C/min, over a range of 40−700 °C.

Results and Discussion

TGA of the samples provided evidence for covalent attachment of functional groups to the nanotube sidewalls as well as quantification for the degree of functionalization. Figure 1 shows TGA plots of p-SWNTs, NO-SWNTs, MA-SWNTs, and COOH-SWNTs. Previous groups have shown that −COOH groups can be covalently bound to the surface using the above described synthesis method.[23] The COOH-SWNTs prepared here show a mass loss of 75.82% versus p-SWNTs over a wide temperature range of approximately 75−700 °C. NO-SWNTs also show a mass loss of 45.17% over 300−700 °C. MA-SWNTs show a significant mass decrease of 38.37% over a shorter temperature range of approximately 150−220 °C. The

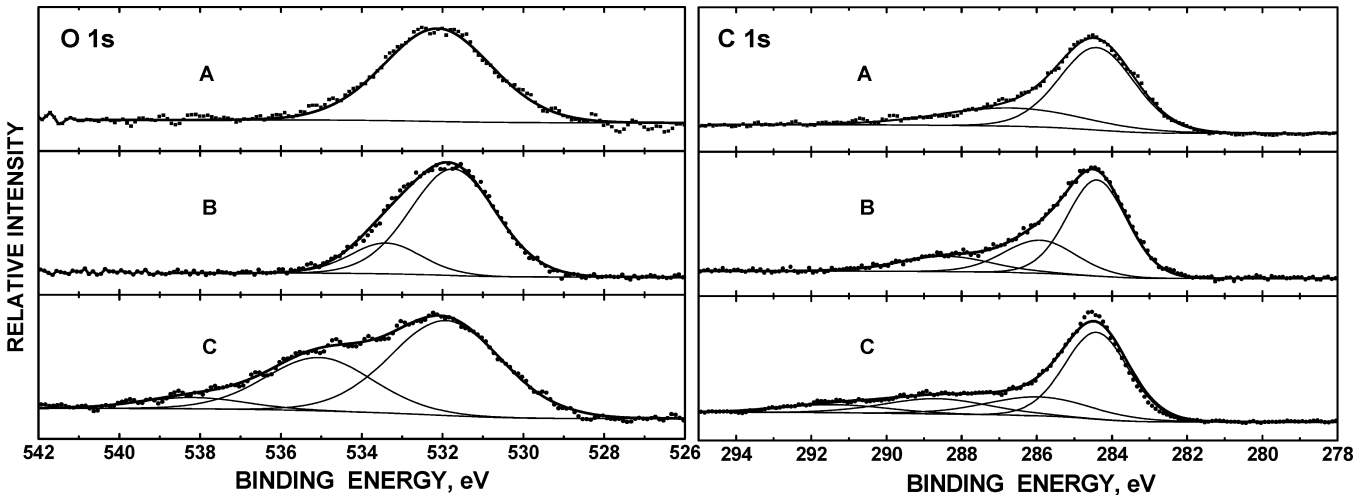

Figure 2. XPS plots of the C 1s (right-hand panel) and O 1s (left-hand panel) core levels of functionalized p-SWNTs: (A) NO-SWNTs; (B) COOH-SWNTs; and (C) MA-SWNTs.

TABLE 1: Summary of XPS Core Level Shifts of Functionalized SWNTs

	C 1s			O 1s			N 1s		
sample	binding energy, eV	fwhm	relative % area, %	binding energy, eV	fwhm	relative % area, %	binding energy, eV	fwhm	relative % area, %
NO-SWNTs	284.4	2.4	70.3	532.1	3.1	100.0	399.5	3.2	82.7
	286.6	4.5	29.7				404.7	2.7	17.3
COOH-SWNTs	284.4	1.9	60.2	531.7	2.5	80.6			
	285.9	2.5	24.9	533.4	2.1	19.4			
	288.4	2.8	14.9						
MA-SWNTs	284.4	2.0	55.6	531.9	3.2	58.2			
	285.9	3.3	19.9	535.1	3.4	37.1			
	288.7	3.3	16.0	538.5	2.4	4.7			
	291.4	3.3	8.5						

sharp mass loss of maleic anhydride groups at a relatively low temperature indicates weaker bonding to the nanowall, which is expected due to the conformational strain required to form a bond between the olefin and the nanotube.[32] However, all functional groups exhibit large mass losses at temperatures in excess of 100 °C. This high temperature mass loss supports the presence of covalent bonding between the functional groups and the tube surface as opposed to the physisorption often seen between oxygen and the nanotube surface. To estimate the surface coverage of functional groups to the SWNT surface, we use the limiting case where all mass loss observed in the TGA (Figure 1) is entirely due to functional group desorption. Mass losses (relative to p-SWNTs) at 700 °C for COOH-, NO-, and MA-SWNTs are 76.1%, 45.0%, and 38.4%, respectively. Accounting for the molar mass of these respective moieties and that of the as-received HiPco p-SWNTs, we estimate the following functional group-to-carbon atom ratios (in parentheses) for each functionalized SWNT to be COOH-SWNTs (1:1.2) > NO-SWNTs (1:3.1) > MA-SWNTs (1:9.6). Calculations for these ratios are included in the Supporting Information.

Surface characterization confirmed the functionalized SWNT structures. Figure 2 shows XPS spectra of the C 1s (right-hand panel) and O 1s (left-hand panel) core levels corresponding to (A) NO-SWNTs, (B) COOH-SWNTs, and (C) MA-SWNTs. The presence of the functional groups are also further verified by the IR data (vide infra). XPS binding energy (BE) peak positions, along with their full-width-at-half-maxima (fwhm) and relative percent area, are tabulated in Table 1. The C 1s peak at BE = 284.4 eV (right-hand panel) is due to the underlying SWNT graphene sheets (Figure 2), which did not undergo functionalization. The spectrum in Figure 3A shows high-resolution narrow scans of the N 1s orbital of the NO-SWNTs. At least chemical oxidation states were observed at 399.5 and 404.7 eV, denoting nitroso (—NO) and nitro ($—NO_2$) structures on the SWNT surface, respectively. The NO oxidation state predominates, making up 82.7% of the overall peak area. The BE peak assignments are in excellent agreement with systematic NO and NO_2 adsorption studies on well-defined surfaces,[33,34] respectively. Physisorbed NO_2 is known to undergo complex transformations (e.g., dimerization, disproportionation, etc.) as it interacts with defect sites on SWNT graphene sheets.[35] No signal from NO_3, known to form from NO_2 decomposition, was observed on the SWNT surface, which would have appeared

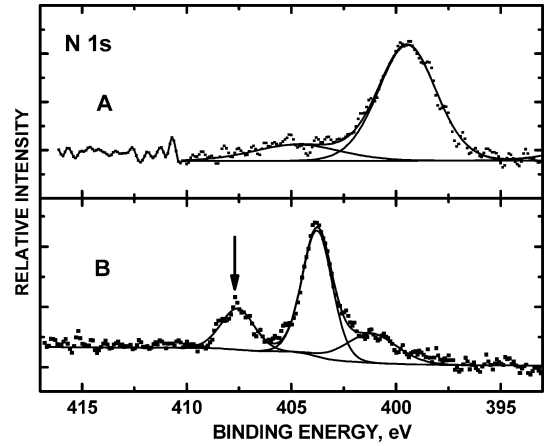

Figure 3. (A) XPS of the N 1s core level for NO-SWNTs; (B) XPS of N 1s of KNO_2 supernatant after electrochemical functionalization; arrow denotes NO_3.

at ~407 eV,[34,36] if present on the sidewalls (Figure 3A). Integrated, deconvoluted peak areas of the N 1s spectrum indicate a 4.7:1 ratio of NO-to-NO_2 surface functional groups. Consistent with this interpretation, the C 1s peak at 286.6 eV (Figure 2A; right) is assigned to the C—N bond adjacent to chemisorbed —N═O. The corresponding O 1s BE peak center at 532.1 eV denotes the oxidation state from —N═O.[37] The spectrum in Figure 3B shows scans of this orbital in the solution supernatant following electrochemical functionalization. A NO_3 oxidation state is clearly seen at ~407.5 eV (denoted by the arrow), accompanying the NO and NO_2 peaks at 401.1 and 403.7 eV,[38] respectively. The NO_2 oxidation state was predominant in the KNO_2 solution.

The C 1s spectral region of the COOH-SWNTs (Figure 2B; right) shows two oxidation states at 285.9 and 288.4 eV, denoting —C—O—[39] and —COO—[39,40] tethered to the SWNTs, respectively. The O 1s spectral region also shows peaks corresponding to hydroxyl (—OH; 531.6 eV) and carboxylic acid (—COOH; 533.2 eV) O atoms tethered to the nanotube surface, matching BE literature values of these groups on carbonaceous surfaces.[41,42] The MA-SWNTs exhibit a series of peaks (Figure 2C) in both the C 1s (right-hand panel) and O 1s (left-hand panel) regions. We assign the 285.9 and 288.7 eV BE peaks in the C 1s region to the C atom, adjacent to the anhydride C—C—O(C═O),[43] and carboxylate —COO—[40] groups of the maleic anhydride, respectively. These chemical oxidation states were also observed in our earlier study involving functionalization of multiwalled carbon nanotubes. We attribute the high BE peak at 291.4 eV to alkyl carbons on the graphene sheet; the BE position is analogous to that for the R—OC(═O)—CH_2—O—R structure reported by Clark et al.[44] In the O 1s region (Figure 2), spectral peaks relate either to —C═O (531.9 eV), or —O—COO— (535.1 eV).[40,45] The assignment of the small O 1s peak at the 538.5 eV BE remains uncertain. They may arise from ether-like structures from which core-ionization energies have been reported in this range.[46]

ATR-IR data provided further validation of the three synthesized SWNT structures. Figure 4A shows the ATR-IR spectrum of the as-received HiPco p-SWNTs. The NO-SWNTs were shown to have —NO groups bonded to their sidewalls by the presence of absorption peaks associated with aromatic nitroso monomer stretching modes (1577 cm^{-1}) and aromatic nitroso cis dimer stretching modes (1411 cm^{-1}, 1360 cm^{-1}) (Figure 4B).[47] Note that a sharp drop in absorbance in the 1550—1450 cm^{-1} is an artifact of the ZnSe crystal background used. Removal of the Triton X-100 surfactant used in the preparation of SWNT sheets for electrochemical nitrosylation was confirmed by taking ATR-IR of the p-SWNT sheet after annealing. Low absorbance at 3200 cm^{-1} corresponding to the surfactant —OH stretch indicates little surfactant was left after annealing (see Supporting Information). The IR spectrum of the COOH-SWNTs shows a broad absorption peak centered at 3128 cm^{-1} that correlates with an ordered OH bond stretch (Figure 4C; inset). It should be noted that no OH features were observed in the MA-SWNTs, NO-SWNTs, or p-SWNTs. This feature is accompanied by a sharp absorption peak at 1734 cm^{-1}, typical for a —C═O stretch in carboxylic acid functionalized SWNTs.[48—50] Presence of the maleic anhydride features in the MA-SWNTs (Figure 4D) is further validated by the IR "double peaks" of the anhydride symmetric and asymmetric stretches at 1740 and 1702 cm^{-1}. The broad feature at 1400—1450 cm^{-1} signifies an acetate structure, while features at 1560 and 1400 cm^{-1} denote the asymmetric —COO—(as) and symmetric —COO—(s) stretches of the carboxylic acids.[49] It should be noted that these symmetric and asymmetric features, along the sharp C═O absorption band at 1734 cm^{-1}, unambiguously denote the presence of carboxylic acid groups absent in our previous nanotube functionalization procedure.[51]

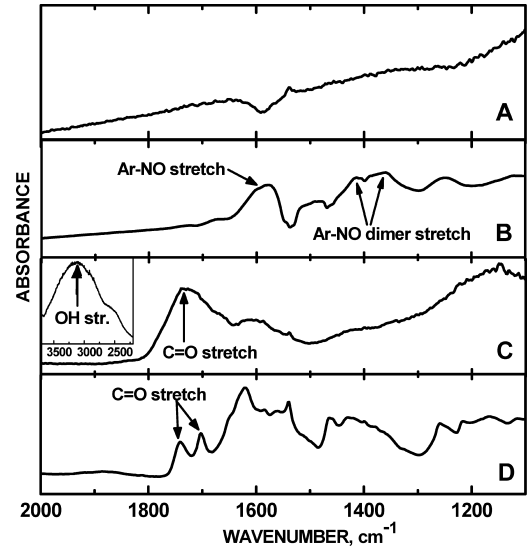

Figure 4. ATR-IR spectra of (A) as-received p-SWNTs; (B) NO-SWNTs; (C) MA-SWNTs; and (D) COOH-SWNTs.

While carboxylic acid functionalization has been studied,[23] maleic anhydride and nitroso functionalizations have yet to be reported. The maleic anhydride reaction is believed to follow the common Diels—Alder pathway.[24,25] TGA confirmed that the covalent linkage between the nanowall and the maleic anhydride formed, and as the mechanism would suggest, this bond was relatively unstable due to the strain produced within the nanowall.

The electrochemical reaction in the nitrite solution leading to nitrosylation is believed to occur via the mechanism described by Piela and Wrona:[52]

$$HNO_2 \rightleftarrows NO_2^- + H^+$$

$$NO_2^- \rightarrow NO_2(g) + e^-$$

$$2NO_2(g) \rightleftarrows N_2O_4(g)$$

$$N_2O_4(g) + H_2O \rightleftarrows HNO_2 + NO_3^- + H^+$$

$$HNO_2 + H_2O \rightarrow 3H^+ + NO_3^- + 2e^-$$

This mechanism accounts for the formation of nitric oxide from nitrite and nitrogen dioxide gas:

$$NO_2(g) + NO_2^- \rightarrow NO_3^- + NO$$

According to this scheme, the nitric oxide would then add onto the SWNT electrode surface. In support of this mechanism, the XPS spectrum of the supernatant clearly showed the presence of NO_3 (Figure 3B, vide supra).

Variations in the measured PZC were observed between the nanotube structures. Figure 5 shows a plot of the values of final

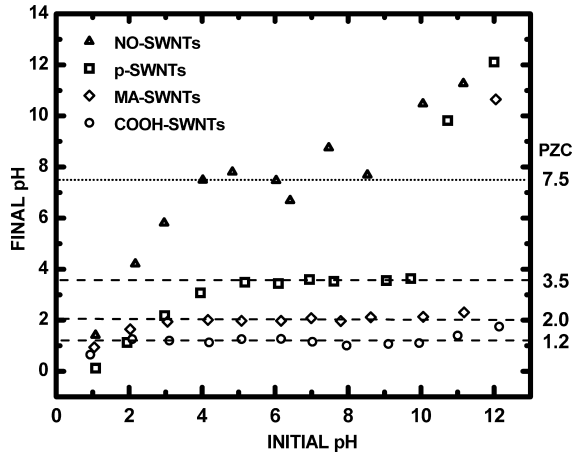

Figure 5. The point of zero charge (PZC) values of NO-SWNTs, p-SWNTs, MA-SWNTs, and COOH-SWNTs are denoted by horizontal lines.

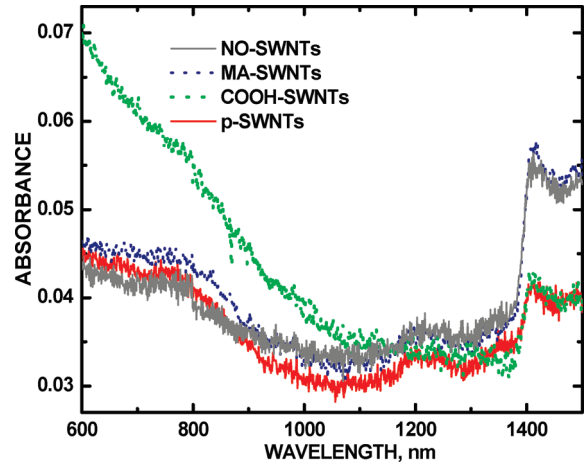

Figure 6. UV−vis-NIR spectra of NO-SWNTs, p-SWNTs, MA-SWNTs, and COOH-SWNTs. Raw unadjusted data is shown.

versus initial pH values of solutions to which various SWNT samples were added. PZC values are denoted by the plateaus (horizontal dashed lines) in the final pH versus initial pH curves. The PZC values in this series of functionalized nanotubes indicate an acidic surface, amenable for adsorption of anionic precursors. The PZC values for the SWNTs are in descending order: NO-SWNTs (7.5) > p-SWNTs (3.5) > MA-SWNTs (2.0) > COOH-SWNTs (1.2). The p-SWNT PZC was found to be somewhat lower compared to other studies,[22] which can be attributed to our use of smaller radius (~0.7 nm) SWNTs. The PZCs were found to be tunable within 6.3 pH units by functionalizing them with various moieties. While the NO moieties raised the PZC, relative to the p-SWNTs, MA and COOH groups lowered it. The COOH groups, due to its acidity, lowered the PZC to a greater degree than the maleic anhydride groups (by 0.8 pH units). We postulate that the moieties affect the PZCs by altering the electron distribution along the SWNT sidewalls. In the context of electrophilic aromatic substitution (EAS) reactions, nitroso groups are known to be electron withdrawing, maleic anhydride groups are lightly electron releasing, and carboxylic acid groups are strongly electron releasing,[53] which can be quantitatively described by its Hammett sigma constant (σ). Since carbon nanotubes are essentially aromatic, peri-condensed benzenoids (composed of sp^2 carbons, arranged in a graphite-like hexagonal pattern) that have aromatic character[54] and have been found to be useful for fabricating hierarchical SWNT structures synthetically,[55] it is appropriate to explore how σ relates to our observed PZC measurements. Also known as the substituent constant, σ determines the effect that a given substituent will have on the equilibrium and rate constants for the disassociation of benzoic acids. The σ parameter takes into account resonance, field, and inductive effects of the substituent. The result is a value whose magnitude gives the relative strength of a substituent's effect on the electronic distribution of a benzoic acid. Standard tables give σ values (for the meta position) of 0.71, 0.39, and 0.35 for nitro, acetoxy, and carboxylic acid groups, respectively.[56,57] Larger σ values denote greater electron-withdrawing character. The MA and COOH groups, which are the least electron withdrawing (i.e., more electron releasing) lowered the PZC, relative to p-SWNTs, while the NO, the most electron withdrawing moiety, raised the PZC. Variations in the electron releasing/withdrawing character of the substituents correlate well with the observed PZC trend. Quantitatively, the σ values of the substituents show the same trend as the experimentally measured PZCs for each of its corresponding functionalized SWNTs. A direct correlation between the σ values of the respective moieties with the corresponding nanotube's PZC was evident.

Density functional theory calculations predict that covalent functionalization of specific moieties to SWNTs would be selective to nanotubes of particular electronic character.[58] Our data is in accord with this theory. Attachment of the NO, MA, and COOH moieties appears to be selective to SWNTs of varying semiconducting character. Figure 6 shows the UV−vis-NIR spectrum for the untreated p-SWNTs in a D_2O colloidal suspension. D_2O solvent was selected to preclude experimental artifacts emanating from interactions with dimethyl formamide (DMF) observable in the 1200−1500 nm region that would interfere with our analysis of the E_{11} band region. However, it should be noted that UV−vis-NIR spectra of the p-SWNTs obtained in DMF (included in the Supporting Information) matches precisely with those reported in the literature for 0.7 nm diameter nanotubes.[59,60] Features the spectra (Figure 6) are due to singularities in the density of states (DOS) and within the 1300−1500 nm region, attributed to band gap transitions in the E_{11} semiconducting nanotubes. The other diagnostic E_{22} region is largely obscured due to solution phase scattering. The greater electron-donating capacity of the moieties, as quantified by σ, the greater the amplitude of the E_{11} transitions. Untreated p-SWNTs (solid line, red trace) at 1500 nm had the lowest amplitude in the series, 0.041 at 1416 nm. This same region in the UV−vis-NIR spectra for the functionalized nanotubes, however, showed an increase from 0.042 to 0.054 to 0.056 at 1416 nm for the attached COOH, NO, and MA nanotube moieties, respectively.

Direct comparison with the as-received p-SWNTs was severely hampered by the marked dissimilarity of the semiconducting E_{11} line shape (solid line, red trace in Figure 6). Increase in the semiconducting E_{11} transition amplitudes showed that moieties with larger σ values had an increasing preference for functionalization to semiconducting nanotubes. However, the association between the relative magnitudes of σ and absorbance in the E_{11} region makes this relation qualitative, and other effects on the preference of functional groups to nanotube type are likely. An analogous phenomenon has been observed with functionalization of diazonium salts having preference for attachment to metallic SWNTs.[61,62] In our series, no correlation of σ with the metallic nanotubes (>800 nm) by UV−vis-NIR was observed. No apparent trend was observed in the E_{11} metallic region (450−650 nm) since scattering effects obscured

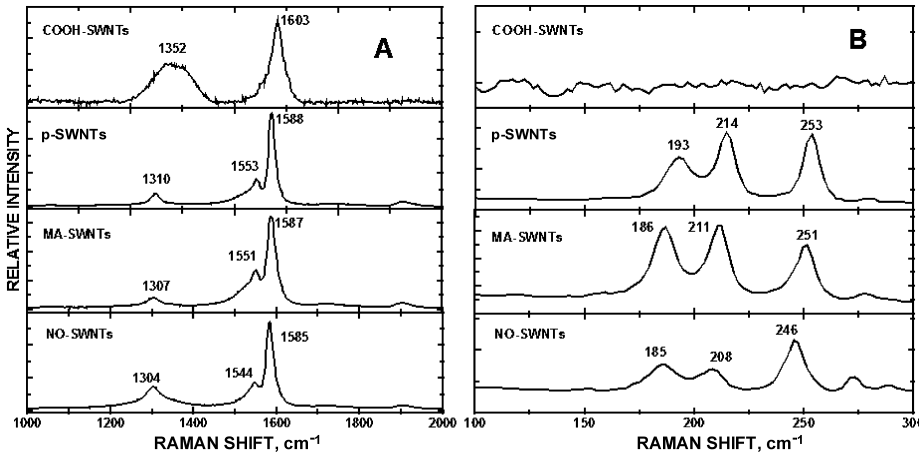

Figure 7. (A) D and G bands in Raman spectra of NO-SWNTs, p-SWNTs, MA-SWNTs, and COOH-SWNTs; (B) radial breathing modes in Raman spectra of NO-SWNTs, p-SWNTs, MA-SWNTs, and COOH-SWNTs.

these features. In the E_{11} semiconducting band structure (Figure 6), however, the amplitudes of NO and MA are clearly greater than for COOH, signifying that the COOH-SWNTs has the least semiconducting character.

Raman spectroscopy provided complementary characterization of the SWNT electronic structure. Raman D and G bands, emanating from disordered and order sp^2-hybridized carbon from the graphene sheets, respectively, is a commonly employed tool for detecting covalent bond formation in SWNTs.[59,63,64] The formation of covalent bonds with metallic nanotubes, in particular, is exhibited in the D band while semiconducting band formation is not. This phenomenon is a consequence of the double resonance process,[65,66] in which metals more easily satisfy resonance conditions (due to zero density of states in the band gap) than semiconducting nanotubes do, thereby resulting in a larger D band feature.[67] On this basis, we infer the degree of functional group covalent bonding to semiconducting nanotubes by examining the relative D-to-G band peak intensities. Figure 7A shows Raman shifts for MA-SWNTs, p-SWNTs, and NO-SWNTs, with D and G bands at ~1310 and ~1590 nm. The Raman shifts appeared at higher frequencies for the COOH-SWNTs at 1352 and 1603 cm^{-1} for the D and G bands, respectively. The D-to-G band ratios (value in parentheses) increased in the following order: NO-SWNTs (0.04398) < MA-SWNTs (0.09128) < p-SWNTs (0.09453) < COOH-SWNTs (0.4342). The lower the D-to-G band ratio, the greater the semiconducting character of the SWNT. This increasing trend of the D-to-G band ratio precisely matches the decreasing order of the E_{11} semiconducting amplitudes of these SWNTs (Figure 6), providing further corroboration that there was covalent functionalization to SWNTs of increasing semiconducting character with greater electron withdrawing capacity of the functional group. The radial breathing mode (RBM) region (Figure 7B) showed differences in the graphene structure in each of the functionalized SWNT surfaces, providing further evidence for covalent attachment of the groups, as opposed to physisorption. The RBM feature at ~185 cm^{-1}, denoting intact single-walled structures, was present in all of the SWNTs, with the exception of those functionalized with COOH. The RBMs on the COOH-SWNT surface were obscured due to the high density of the moieties tethered to the sidewalls and/or introduction of surface defects.

Trends in the UV−vis-NIR and Raman spectral data are in good agreement with first principle *ab initio* calculations, which have shown that sidewall functionalization to SWNTs significantly alters the semiconducting band structure[68] such that in aqueous solution, surface protonation is hampered, resulting in a higher PZC. It should be noted, however, that the particularly harsh acid conditions (absent in NO and MA functionalization) used to create the COOH-SWNTs likely damaged the graphene sheets. As a result, the D-band intensity is broadened and enhanced (from an increase in the disordered sp^3-hybridized carbon), resulting in the relatively high D-to-G band ratio for COOH-SWNTs.

In summary, we have altered the PZC of HiPco SWNTs within a range of 6.3 pH units using chemical functionalization. Increasing electron withdrawing character resulted in higher PZC values. Increasing electron withdrawing character of the moiety seems to show general selectivity for covalent attachment to SWNTs of greater semiconducting character, as observed in the UV−vis-NIR and Raman spectra. The greater the semiconducting character of the SWNTs, the higher the PZC. It should be noted that this correlation is by no means direct. Pronounced band structures, observed in both the UV−vis-NIR and Raman spectra, indicate two possible scenarios for their origin: (i) There is an increasing selectivity for semiconducting SWNTs with moieties with increasing σ values and/or (ii) covalent attachment of the SWNTs with moieties of increasing σ values augments the SWNT semiconducting structure. Since no electronic separation procedures were implemented, it appears that scenario (ii) plays a significant role. Dependence of PZC on the electronic character of the SWNTs, which can be altered via chemical functionalization, is an important factor to consider when fabricating SWNT architectures from aqueous solution.

Acknowledgment. MRM gratefully acknowledges support from the Opportunities for Undergraduate Research (OURE) at Missouri University of Science and Technology. We thank Dr. Jay Switzer for permitting us the use of the Cary 5 UV-vis-NIR instrument and potentiostat in his laboratory. We also thank Drs. Jong Wook Lim and Eric Bohannan of the Materials Research Center at Missouri S&T for assistance in the Raman spectroscopy and TGA, respectively. This work was funded by the University of Missouri Research Board (Grant RBJ61) and the Foundation for Chemical Research, Inc., Rolla, MO.

Supporting Information Available: Additional information showing removal of the Triton X-100 surfactant from the SWNTs prior to electrochemical functionalization, the UV−vis-NIR spectrum of the as-received p-SWNTs in dimethyl formamide solvent, and calculations estimating the coverage of functional groups tethered to the SWNTs based on mass loss

obtained from TGA data are included. This material is available free of charge via the Internet at http://pubs.acs.org.

References and Notes

(1) Sherigara, B. S.; Kutner, W.; D'Souza, F. Electrocatalytic properties and sensor applications of fullerenes and carbon nanotubes. *Electroanalysis* **2003**, *15*, 253–772.

(2) Zhang, Y.; Li, J.; Shen, Y.; Wang, M.; Li, J. Poly-L-Lysine functionalization of single-walled carbon nanotubes. *J. Phys. Chem. B* **2004**, *108*, 15343–15346.

(3) Poh, W. C.; Loh, K. P.; Zhang, W. D.; Triparthy, S.; Ye, J.-S.; Sheu, F.-S. Biosensing properties of diamond and carbon nanotubes. *Langmuir* **2004**, *20*, 5484–5492.

(4) Valentini, F.; Orlanducci, S.; Terranova, M. L.; Amine, A.; Palleschi, G. Carbon nanotubes as electrode materials for the assembling of new electrochemical biosensors. *Sens. Actuators, B* **2004**, *B100*, 117–125.

(5) Planeix, J. M.; Coustel, N.; Coq, B.; Brotons, V.; Kamblar, P. S.; Dutartre, R.; Geneste, P.; Bernier, P.; Ajayan, P. M. Application of carbon nanotubes as supports in heterogeneous catalysis. *J. Am. Chem. Soc.* **1994**, *116*, 7935–7936.

(6) Freemantle, M. *Chem. Eng. News* **1996**, *74*, 62.

(7) Che, G.; Lakshmi, B. B.; Fisher, E. R.; Martin, C. R. Carbon nanotubule membranes for electrochemical energy storage and production. *Nature* **1998**, *393*, 346–349.

(8) Che, G.; Lakshmi, B. B.; Martin, C. R.; Fisher, E. R. Metal-nanocluster-filled carbon nanotubes: catalytic properties and possible applications in electrochemical energy storage and production. *Langmuir* **1999**, *15*, 750–758.

(9) Li, W.; Liang, C.; Qiu, J.; Zhou, W.; Han, H.; Wei, Z.; Sun, G.; Xin, Q. Carbon nanotubes as supports for cathode catalyst of a direct methanol fuel cell. *Carbon* **2002**, *40*, 791–794.

(10) Yoshitake, T.; Shimakawa, S.; Kimura, H.; Ichihashi, T.; Kubo, Y.; Kasuya, D.; Yakahashi, K.; Kokai, F.; Yudasaka, M.; Iijima, S. Preparation of fine platinum catalyst supported on single-wall carbon nanohorns for fuel cell application. *Physica B* **2002**, *323*, 124–126.

(11) Gennett, T.; Landi, B. J.; Elich, J. M.; Jones, K. M.; Alleman, J. L.; Lamarre, P.; Morris, R. S.; Raffaelle, R. P.; Heben, M. J. Fuel cell applications of nanotube-metal supported catalysts. *Mater. Res. Soc. Symp. Proc.* **2003**, *756*, 379–384.

(12) Gangeri, M.; Perathoner, S.; Centi, G. Synthesis and performances of carbon-supported nobel metal nanoclusters as electrodes for polymer electrolyte membrane fuel cells. *Inorg. Chim. Acta* **2006**, *359*, 4828–4832.

(13) Brown, G. E., Jr.; Henrich, V. E.; Casey, W. H.; Clark, D. L.; Eggleston, C.; Felmy, A.; Goodman, D. W.; Grätzel, M.; Maciel, G.; McCarthy, M. I.; Nealson, K. H.; Sverjensky, D. A.; Toney, M. F.; Zachara, J. M. Metal oxide surfaces and their interactions with aqueous solutions and microbial organisms. *Chem. Rev.* **1999**, *99*, 77–174.

(14) Leon y Leon, C. A.; Solar, J. M.; Calemma, V.; Radovic, L. R. Evidence for the protonation of basal plane sites on carbon. *Carbon* **1992**, *30*, 797–811.

(15) Sepulveda-Escribano, A.; Coloma, F.; Rodriguez-Reinoso, F. Platinum catalysts supported on carbon blacks with different surface chemical properties. *Appl. Catal., A: Gen.* **1998**, *173*, 247–257.

(16) Figueiredo, J. L.; Pereira, M. F. R.; Freitas, M. M. A.; Orfao, J. J. M. Modification of the surface chemistry of activated carbons. *Carbon* **1999**, *37*, 1379–1389.

(17) Fraga, M. A.; Jordao, E.; Mendes, M. J.; Freitas, M. M. A.; Faria, J. L.; Figueiredo, J. L. Properties of carbon-supported platinum catalysts: role of carbon surface sites. *J. Catal.* **2002**, *209*, 355–364.

(18) Hao, X.; Quach, L.; Korah, J.; Spieker, W. A.; Regalbuto, J. R. The control of platinum impregnation by PZC alteration of oxides and carbon. *J. Mol. Catal., A* **2004**, *219*, 97–107.

(19) Iijima, S. Helical microtubules of graphitic carbon. *Nature* **1991**, *354*, 56–58.

(20) Hamada, N.; Sawada, S.; Oshiyama, A. New one-dimensional conductors: graphitic microtubules. *Phys. Rev. Lett.* **1992**, *68*, 1579–1581.

(21) Maldonado, S.; Morin, S.; Stevenson, K. J. Electrochemical oxidation of catecholamines and catechols at carbon nanotube electrodes. *Analyst* **2006**, *131*, 262–267.

(22) Matarredona, O.; Rhoads, H.; Li, Z.; Harwell, J. H.; Balzono, L.; Resasco, D. E. Dispersion of single-walled carbon nanotubes in aqueous solutions of the anionic surfactant NaDDBS. *J. Phys. Chem. B* **2003**, *107*, 13357–13367.

(23) Lu, X.; Imae, T. Size-controlled in situ synthesis of metal nanoparticles on dendrimer-modified carbon nanotubes. *J. Phys. Chem. C* **2007**, *111*, 2416–2420.

(24) Wang, Y. B.; Malhotgra, S. V.; Owens, F. J.; Iqbal, Z. Electrochemical nitration of single-wall carbon nanotubes. *Chem. Phys. Lett.* **2005**, *407*, 68–72.

(25) Sauer, J.; Wiest, H.; Milert, A. Diels-Alder reaction. I. Reactivity of dienophiles towards cyclopentadiene and 9,10-dimethylanthracene. *Chem. Ber.* **1964**, *97*, 3183–3207.

(26) Dewar, M. J. S.; Pyron, R. S. Nature of the transition state in some Diels-Alder reactions. *J. Am. Chem. Soc.* **1970**, *92*, 3098–3103.

(27) Mercuri, F.; Sgamellotti, A. First-principles investigations on the functionalization of chiral and non-chiral carbon nanotubes by Diels-Alder cycloaddition reactions. *Phys. Chem. Chem. Phys.* **2009**, *11*, 563–567.

(28) Suzuki, S.; Watanabe, Y.; Ogino, T.; Heun, S.; Gregoratti, L.; Barinov, A.; Kaulich, B.; Kiskinova, M. Electronic structure of carbon nanotubes studied by photoelectron spectroscopy. *Phys. Rev. B* **2002**, *66*, 8119–8121.

(29) Ago, H.; Kugler, T.; Franco, C.; Salaneck, W. R.; Shaffer, M., S. P.; Windle, A. H.; Friend, R. H. Work functions and surface functional groups of multiwall carbon nanotubes. *J. Phys. Chem. B* **1999**, *103*, 8116–8121.

(30) Shirley, D. A. High-resolution X-ray photoemission spectrum of the valence bands of gold. *Phys. Rev. B* **1972**, *5*, 4709–4714.

(31) Park, J.; Regalbuto, J. R. A simple, accurate determination of oxide PZC and the strong buffering effect of oxide surfaces at incipient wetness. *J. Colloid Interface Sci.* **1995**, *175*, 239–252.

(32) Lu, X.; Tian, F.; Wang, N.; Zhang, Q. Organic functionalization of the sidewalls of carbon nanotubes by Diels-Alder reactions: a theoretical prediction. *Org. Lett.* **2002**, *4*, 4313–4315.

(33) Rodriguez, J. A.; Jirsak, T.; Dvorak, J.; Sambasivan, S.; Fischer, D. Reaction of NO_2 with Zn and ZnO: photoemission, XANES, and density functional studies of the formation of NO_3. *J. Phys. Chem. B* **2000**, *104*, 319–328.

(34) Schmitz, P. J.; Baird, R. J. NO and NO_2 adsorption on barium oxide: model study of the trapping stage of NO_x conversion via lean NO_x traps. *J. Phys. Chem. B* **2002**, *106*, 4172–4180.

(35) Goldoni, A.; Larciprete, R.; Petaccia, L.; Lizzit, S. Single-wall carbon nanotube interaction with gases: sample contaminants and environmental monitoring. *J. Am. Chem. Soc.* **2003**, *125*, 11329–11333.

(36) Torres, J.; Perry, C. C.; Bransfield, S. J.; Fairbrother, D. H. Low-temperature oxidation of nitrided iron surfaces. *J. Phys. Chem. B* **2003**, *107*, 5558–5567.

(37) Batich, C. D.; Donald, D. S. X-ray photoelectron spectroscopy of nitroso compounds: relative ionicity of the closed and open forms. *J. Am. Chem. Soc.* **1984**, *106*, 2758–2761.

(38) Aduru, S.; Contarini, S.; Rabalais, J. W. Electron-, X-ray-, and ion-stimulated decomposition of nitrate salts. *J. Phys. Chem.* **1986**, *90*, 1683–1688.

(39) Blanchard, N. P.; Hatton, R. A.; Silma, S. R. P. Tuning the work function of surface oxidized multi-wall carbon nanotubes via cation exchange. *Chem. Phys. Lett.* **2007**, *434*, 92–95.

(40) Xing, Y.; Li, L.; Chusuei, C. C.; Hull, R. V. Sonochemical oxidation of multiwalled carbon nanotubes. *Langmuir* **2005**, *21*, 4185–4190.

(41) Blyth, R. I. R.; Buqa, H.; Netzer, F. P.; Ramsey, M. G.; Besenhard, J. O.; Golob, P.; Winter, M. XPS studies of graphite electrode materials for lithium ion batteries. *Appl. Surf. Sci.* **2000**, *167*, 99–106.

(42) Wildgoose, G. G.; Lawrence, N. S.; Leventis, H. C.; Jiang, L.; Jones, T. G. J.; Compton, R. G. X-ray photoelectron spectroscopy studies of graphite powder and multiwalled carbon nanotubes covalently modified with Fast Black K: evidence for a chemical release mechanism via electrochemical reduction. *J. Mater. Chem.* **2005**, *15*, 953–959.

(43) Evenson, S. A.; Badyal, J. P. S. Solventless attachment of long-chain molecules to poly(ethylene-alt-maleic anhydride) copolymer surfaces. *J. Phys. Chem. B* **1998**, *102*, 5500–5502.

(44) Clark, D. T.; Feast, W. J.; Tweedale, P. J.; Thomas, H. R. ESCA applied to polymers. XXVI. Investigation of a series of aliphatic, aromatic and fluorine-containing polycarbonates. *J. Polym. Sci. Polym. Chem. Ed.* **1980**, *18*, 1651–1654.

(45) Ota, H.; Sakata, Y.; Inoue, A.; Yamaguchi, S. Analysis of vinylene carbonate derived SEI layers on graphite anode. *J. Electrochem. Soc.* **2004**, *151*, A1659–A1669.

(46) Siggel, M. R. F.; Thomas, T. D. Linear correlation of oxygen core-ionization energies of alcohols and acids with those of the corresponding methyl and ethyl ethers and esters. *J. Electron Spectrosc. Relat. Phenom.* **1989**, *48*, 101–116.

(47) Smith, A. L. *Applied Infrared Spectroscopy*; Wiley and Sons: New York, 1979.

(48) Mawhinney, D. B.; Naumenko, V.; Yates, J. T.; Liu, J.; Smalley, R. E. Enhancement of adsorption inside of single-walled nanotubes: opening the entry ports. *Chem. Phys. Lett.* **2000**, *321*, 292–296.

(49) Petroski, J.; El-Sayed, M. A. FTIR study of the adsorption of the capping material to different platinum nanoparticle shapes. *J. Phys. Chem. A* **2003**, *107*, 8371–8375.

(50) Zhang, J.; Hongling, Z.; Qing, Q.; Yang, Y.; Li, Q.; Liu, Z.; Guo, X.; Du, Z. Effect of chemical oxidation on the structure of single-walled nanotubes. *J. Phys. Chem. B* **2003**, *107*, 3712–3718.

(51) Hull, R. V.; Li, L.; Xing, Y.; Chusuei, C. C. Pt nanoparticle binding on functionalized carbon nanotubes. *Chem. Mater.* **2006**, *18*, 1780–1788.

(52) Piela, B.; Wrona, P. K. Oxidation of nitrites on solid electrodes. I. Determination of the reaction mechanism on the pure electrode surface. *J. Electrochem. Soc.* **2002**, *149*, E55–E63.

(53) Smith, M. B. *Organic Synthesis*, 2nd ed.; McGraw Hill: Boston, MA, 2002.

(54) Lukovits, I.; Kármán, F.; Nagy, P. M.; Kálmán, E. Aromaticity of carbon nanotubes. *Croat. Chem. Acta* **2007**, *80*, 233–237.

(55) Zorbas, V.; Smith, A. L.; Xie, H.; Ortiz-Acevedo, A.; Dalton, A. B.; Dieckmann, G.; Draper, R. K.; Baughman, R. H.; Musselman, I. H. Importance of aromatic content for peptide/single-walled carbon nanotube interactions. *J. Am. Chem. Soc.* **2005**, *127*, 12323–12328.

(56) Hansch, C.; Leo, A.; Taft, R. W. A survey of Hammett substituent constants and resonance and field parameters. *Chem. Rev.* **1991**, *91*, 165–195.

(57) Carey, F. A. *Advanced Organic Chemistry, Part A: Structure and Mechanisms*, 4th ed.; Kluwer Academics/Plenum Publishers: New York, 2002.

(58) Tasis, D.; Tagmatarchis, N.; Bianco, A.; Prato, M. Chemistry of carbon nanotubes. *Chem. Rev.* **2006**, *106*, 1105–1136.

(59) Bahr, J. L.; Yang, J.; Kosynkin, D. V.; Bronikowski, M. J.; Smalley, R. E.; Tour, J. M. Functionalization of carbon nanotubes by electrochemical reduction of aryl diazonium salts: a bucky paper electrode. *J. Am. Chem. Soc.* **2001**, *123*, 6536–6542.

(60) Bahr, J. L.; Tour, J. M. Covalent chemistry of single-wall carbon nanotubes. *J. Mater. Chem.* **2002**, *12*, 1952–1958.

(61) Strano, M. S.; Dyke, C. A.; Usrey, M. L.; Barone, P. W.; Allen, M. J.; Shan, H.; Kittrell, C.; Hauge, R. H.; Tour, J. M.; Smalley, R. E. Electronic structure control of single-walled carbon nanotube functionalization. *Science* **2003**, *301*, 1519–1522.

(62) Strano, M. S.; Huffman, C. B.; Moore, V. C.; O'Connell, M. J.; Haroz, E. H.; Hubbard, J.; Miller, M.; Rialon, K.; Kittrell, C.; Ramesh, S.; Hauge, R. H.; Smalley, R. E. Reversible, band-gap-selective protonation of single-walled carbon nanotubes in solution. *J. Phys. Chem. B* **2003**, *107*, 6979–6985.

(63) Holzinger, M.; Abraham, J.; Whelan, P.; Graupner, R.; Ley, L.; Hennrich, F.; Kappes, M.; Hirsch, A. Functionalization of single-walled carbon nanotubes with (R-)oxycarbonyl nitrenes. *J. Am. Chem. Soc.* **2003**, *125*, 8566–8580.

(64) Simmons, J. M.; Nichols, B. M.; Baker, S. E.; Marcus, M. S.; Castellini, O. M.; Lee, C.-S.; Hamers, R. J.; Eriksson, M. A. Effect of ozone oxidation on single-walled carbon nanotubes. *J. Phys. Chem. B* **2006**, *110*, 7113–7118.

(65) Maultzch, J.; Reich, S.; Thomsen, C. Chirality-selective Raman scattering of the D mode in carbon nanotubes. *Phys. Rev. B* **2001**, *64*, 121407−1121407−4.

(66) Zólyomi, V.; Kürti, J.; Grüneis, A.; Kuzmany, H. Origin of the fine structure of the Raman D band in single-wall carbon nanotubes. *Phys. Rev. Lett.* **2003**, *90*, 157401-1–157401-4.

(67) Abdula, D.; Nguyen, K. T.; Shim, M. Raman spectral evolution in individual metallic single-walled carbon nanotubes upon covalent sidewall functionalization. *J. Phys. Chem. C* **2007**, *111*, 17755–17760.

(68) Pan, H.; Feng, Y. P.; Lin, J. Y. Ab initio study of OH-functionalized single-wall carbon nanotubes. *Phys. Rev. B* **2004**, *70*, 245425-1–245425-5.

JP901439G

Supporting Information

Charging Nanowalls: Adjusting the Carbon Nanotube Isoelectric Point via Surface Functionalization

*Martin R. McPhail, Jacob A. Sells, Zhen He and Charles C. Chusuei**

Chemistry Department, Missouri University of Science and Technology, 142 Schrenk Hall, 400 West 11th Street, Rolla, MO 65409-0010 USA

CORRESPONDING AUTHOR. *E-mail: chusuei@mst.edu

Total of 3 pages, 2 figures and 3 calculations.

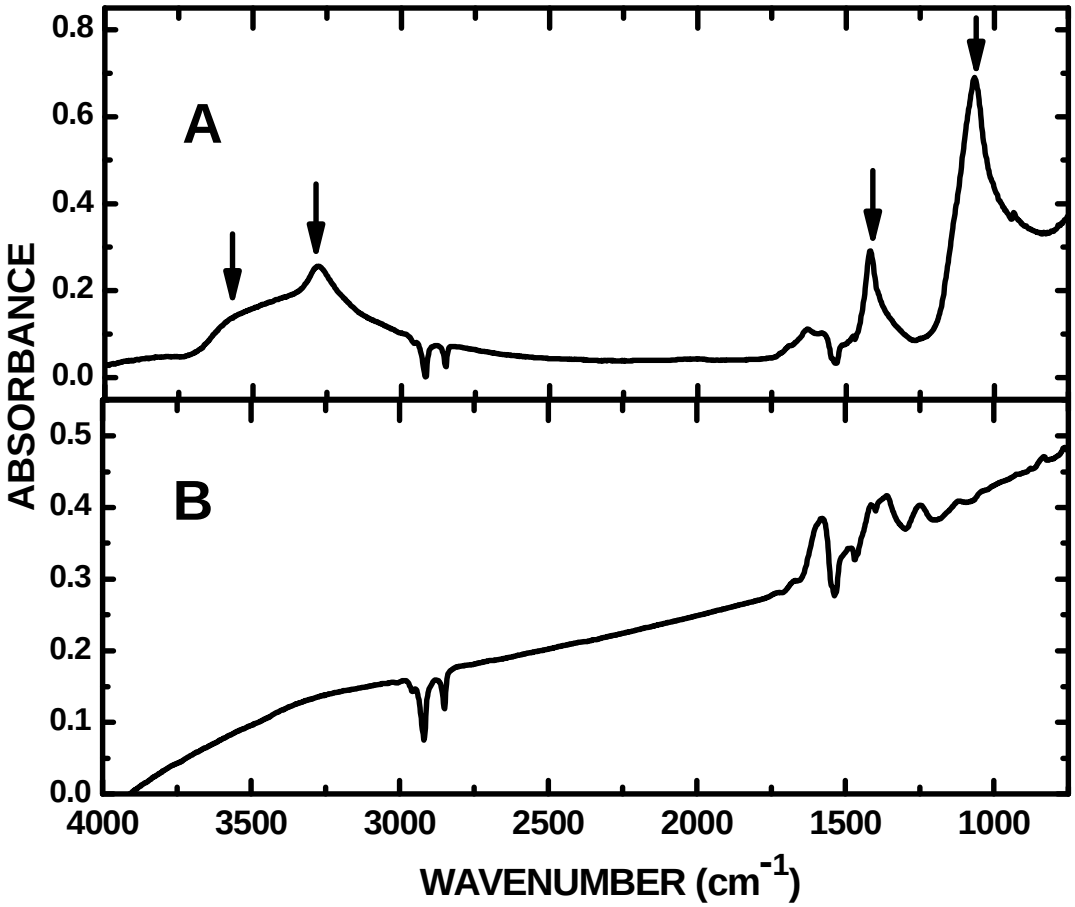

Figure S1: ATR-IR spectra of **(A)** Triton X-100 treated SWNTs annealed to 120°C for 2 hr, 300°C for 1hr and 800°C for 30 min.(arrows denote peaks due to Triton X-100); and **(B)** these same SWNTs after electrochemical nitrosylation.

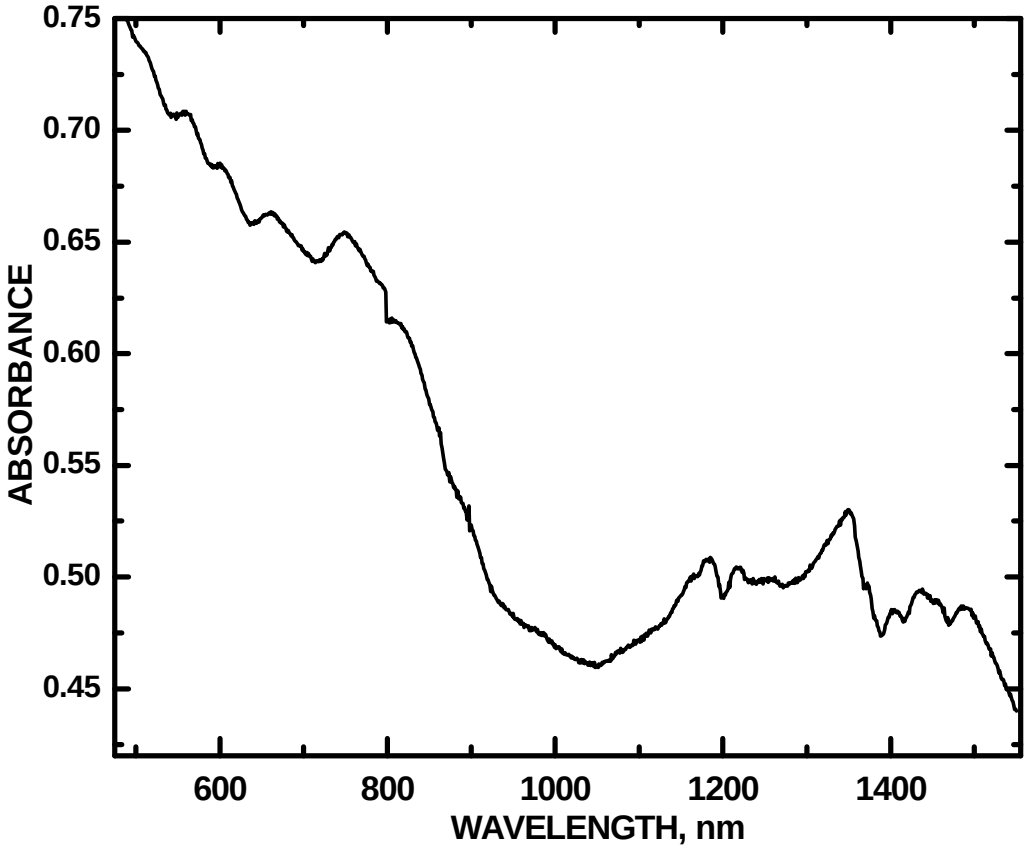

Figure S2: UV-vis-NIR spectrum of as-received 0.7 nm diameter p-SWNTs as a colloidal suspension in dimethyformamide. There is a discontinuity in the absorbance spectrum at 798 nm of less than 0.030 units due to sensitivity changes in the instrument.

Estimating the coverage of tethered functional groups to the SWNT surface:

(1) For the COOH-SWNTs, there was a 76.1% mass loss observed due to functional group desorption relative to p-SWNTs.

molar mass of COOH = 45.018 amu

molar mass of SWNTs = 2.77 x 10^6 g/mol or 2.31 x 10^5 carbon atoms

The number of functional groups present, x, can be determined by:

$$\frac{(x)\cdot(45.018 amu)}{(2.31x10^5\, atoms)\cdot(12.011 amu)} = \frac{76.1\%}{23.9\%}$$ ➔ x = 1.96x10^5 COOH functional groups

Estimating the coverage of tethered functional groups to the SWNT surface: (continued)

Therefore, the ratio of –COOH groups to carbon atoms is:

$$\frac{(2.31x10^5 C \quad atoms)}{(1.96x10^5 COOH \quad groups)} \rightarrow$$ 1.2:1 or 1 COOH group per 1.2 carbon atoms.

(2) For the NO-SWNTs, there was a 45.0% mass loss observed due to functional group desorption relative to p-SWNTs.

molar mass of NO = 30.006 amu

molar mass of SWNTs = 2.77 x 10^6 g/mol or 2.31 x 10^5 carbon atoms

The number of functional groups present, x, can be determined by:

$$\frac{(x)\cdot(30.006amu)}{(2.31x10^5 atoms)\cdot(12.011amu)} = \frac{45.0\%}{55.0\%} \rightarrow$$ x = 7.56x10^4 NO functional groups

Therefore, the ratio of NO groups to carbon atoms is:

$$\frac{(2.31x10^5 C \quad atoms)}{(7.56x10^4 NO \quad groups)} \rightarrow$$ 3.1:1 or 1 NO group per 3.1 carbon atoms.

(3) For the MA-SWNTs, there was a 38.4% mass loss observed due to functional group desorption relative to p-SWNTs.

molar mass of MA = 72.020 amu

molar mass of SWNTs = 2.77 x 10^6 g/mol or 2.31 x 10^5 carbon atoms

The number of functional groups present, x, can be determined by:

$$\frac{(x)\cdot(72.020amu)}{(2.31x10^5 atoms)\cdot(12.011amu)} = \frac{38.4\%}{61.6\%} \rightarrow$$ x = 2.40x10^4 MA functional groups

Therefore, the ratio of carbon atoms to MA groups is:

$$\frac{(2.31x10^5 C \quad atoms)}{(2.40x10^4 MA \quad groups)} \rightarrow$$ 9.6:1 or 1 MA group per 9.6 carbon atoms.